# Chapter 11
# Real-Time Regional Ionospheric Total Electron Content Modeling Using Spherical Harmonic Function

**Shoujian Zhang, Xin Chang and Wei Zhang**

**Abstract** The Ionospheric Total Electron Content (TEC) model is very important for navigation, precise positioning and some other applications. In recent years, with the fast development of the local Continuously Operating Reference Stations (CORS) in China, determining precise local Ionospheric TEC model is very attractive for local precise positioning. Ionosphere delay is one of the most error sources. At present, the establishment of large-scale CORS system in china provided the conditions for establish real-time regional Ionospheric model using spherical harmonic function. In this paper, we will model the ionospheric TEC using the GPS geometry-free combination observable with the low order spherical harmonic function, meanwhile, the DCBs will also be solved with the Vertical TEC (VTEC). In the experiment, about 20 IGS stations from Europe are chosen to simulate a CORS network, a set of ionosphere coefficients is assumed every 2 h. By comparisons with the IGS Analysis Centre's model, it shows that the mean difference of the DCBs is less than 0.35 ns with the RMS about 0.2 ns, and the difference of the VTEC is less than 3 TECU.

**Keywords** CORS · Ionosphere · Regional · Modeling · TEC · DCB

## 11.1 Introduction

Ionosphere total electron content (TEC) and its change are not only the important materials of the morphological study of the ionosphere but also the important parameters of the ionosphere corrections for precise positioning, navigation and radio science. After the revoking of SA policy, ionospheric delay has become the

S. Zhang (✉) · X. Chang · W. Zhang
School of Geodesy and Geomatics, Wuhan University, Wuhan, China
e-mail: shjzhang@sgg.whu.edu.cn

J. Sun et al. (eds.), *China Satellite Navigation Conference (CSNC) 2013 Proceedings*, Lecture Notes in Electrical Engineering 243,
DOI: 10.1007/978-3-642-37398-5_11, 

largest error source for positioning and navigation. In precision positioning, the precise estimation of ionosphere not only helps to improve the quality of GNSS observation, but also exerts significant meaning in the research of atmosphere and earth observation [1, 2]. In the recent ten years, International GNSS Service has adopted the formatted file of IONEX proposed by Schaer [3], and has launch some ionosphere products like the global ionosphere map (GIM), the hardware delay of GPS etc. An intensive study on building the model of ionosphere delay through the GPS observation data has been made by Zhang Xiaohong et al. [4]. Some experts, including Yuan [5] and Jikun Ou, have put forward the law about the delay of ionosphere and the variation of electron density based on the GPS. Zhang [6] has made a comparison between different ionosphere models.

The Continuously Operating Reference Station (CORS) can provide not only the real-time precise positioning results, but also the atmosphere and ionosphere information of the coverage area. The high precision real-time ionosphere model, based on the regional CORS network, has important implications for improving the positioning results of the single-frequency receivers, network RTK and other precise positioning. This paper advances the regional model using the fourth-order spherical harmonics. The estimation of the total electron content (TEC) was seriously affected by the DCBs, when conducting the ionosphere modelling in the use of combination observations. At present only part of the IGS tracking station DCBs products of the global model can be taken into account, so the P1 to P2 DCBs can be accurately estimated in the this paper. Considering the DCBs do not change within a day, the authors can separate the VTEC and establish the real-time regional spherical harmonic model. After comparison and analysis, the estimates

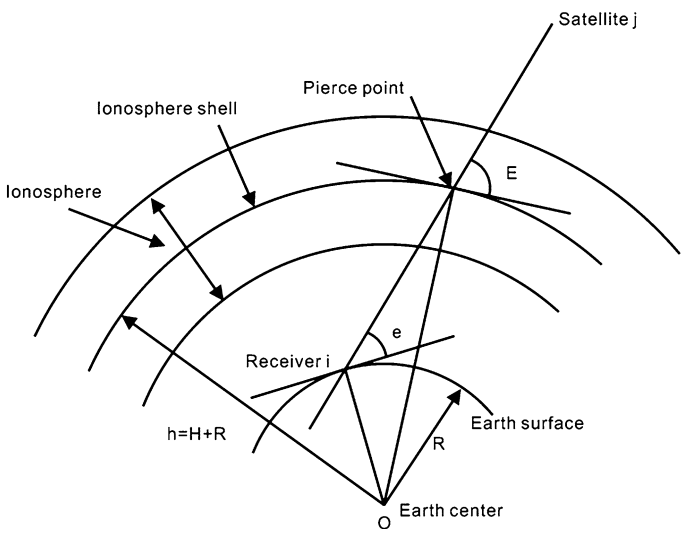


**Fig. 11.1** Ionosphere shell

from this paper show good agreement with the IGS Analysis Centres with a mean difference of less than 0.35 ns and an RMS of less than 0.2 ns, a VTEC of less than 3 TECU, and it can much more perfectly reflect the TEC distribution in regional area.

## 11.2 GPS Ionosphere Measurements

Ionosphere is a region which is composed of ionized plasma and extends from roughly 50 to 2,000 km above the surface of the earth. Generally, the ionosphere can be divided into several layers according to electron density, which reaches its peak value at about 350 km in altitude. For 2D ionosphere modeling, ionosphere shell model is usually applied, as shown in Fig. 11.1 [7]. The ionosphere is assumed to be concentrated on a spherical shell of infinitesimal thickness located at the altitude of H above the earth's surface which is described by total electron content (TEC). TEC is a total number of free electrons in a cylinder with a bottom area of 1 $m^2$, which is usually represented by TECU (1TECU = $10^{16}$ Ne/$m^2$).

A dual-frequency GPS receiver has both code and carrier phase observations on $L_1$ (1,575.42 MHz) and $L_2$ (1,227.60 MHz) frequencies. Mathematically the corresponding observations can be described as [8]

$$P^i_{k,j} = \rho^i_{0,j} + d^i_{ion,k,j} + d^i_{trop,j} + c(\tau^i - \tau_j) + d^i_k + d_{k,j} + \varepsilon^i_{P,k,j} \tag{11.1}$$

$$\begin{aligned} L^i_{k,j} =& \rho^i_{0,j} + d^i_{ion,k,j} + d^i_{trop,j} + c(\tau^i - \tau_j) - \lambda\left(b^i_{k,j} + N^i_{k,j}\right) \\ &+ \varepsilon^i_{L,k,j} \end{aligned} \tag{11.2}$$

where $P$ is the pseudorange observation, $L$ is the carrier phase observation, $\rho$ is the true geometric range between receiver and satellite (m), $d_{ion}$ is the ionosphere delay (m), $d_{trop}$ is the troposphere delay (m), $c$ is the speed of light (m/s), $\tau^i$ is the satellite clock error with respect to GPS time (s), $\tau_j$ is the receiver clock error with respect to GPS time (s), $d$ is the code delays for satellite and receiver instrument bias (m), $b$ is the phase advance of the satellite and receiver instrument bias, $N$ is the ambiguity of the carrier phase, $\varepsilon$ is the residual in the GPS measurements, the subscript $k$ (= 1, 2) stands for the frequency, the superscript $i$ stands for the sequence number of the GPS satellite, and the subscript $j$ stands for the sequence number of the GPS receiver.

Through difference with dual-frequency observations, the ionosphere delays can be obtained through the following equations:

$$P_4 = P^i_{1,j} - P^i_{2,j} = \left(d^i_{ion,1,j} - d^i_{ion,2,j}\right) + DCB^i + DCB_j \tag{11.3}$$

$$\begin{aligned} L_4 &= L^i_{1,j} - L^i_{2,j} \\ &= -(d^i_{ion,\,1,j} - d^i_{ion,\,2,j}) - \lambda(b^i_{1,j} - b^i_{2,j}) - \lambda(N^i_{1,j} - N^i_{2,j}) \end{aligned} \tag{11.4}$$

where $DCB^i = d^i_1 - d^i_2$, and $DCB_j = d_{1,j} - d_{2,j}$ stand for differential code bias of the satellite and receiver which is the delay of $P_1$ relative to $P_2$. As $P_4$ has larger noise, $L_4$ is used to smooth the $P_4$. Cycle slips and gross errors in the carrier phase observations should be removed before smoothing the $P_4$, both Melbourne-Wübbena combination (MW) and ionosphere residual observations are used to detect cycle slips and gross errors. The following equations are utilized in the smoothing of the $P_4$:

$$\begin{aligned} P_{4,\,s} = &\frac{(\omega_1)_t}{(\omega_1)_t + (\omega_2)_t}(P_4)_t + \frac{(\omega_2)_t}{(\omega_1)_t + (\omega_2)_t} \\ &[(P_{4,\,s})_{t-1} + \delta(L_4)_{t,\,t-1}] \end{aligned} \tag{11.5}$$

$$(\omega_1)_t = \frac{1}{\sigma^2_{(P_4)_t}} \tag{11.6}$$

$$(\omega_2)_t = \frac{1}{\sigma^2_{(P_4)_t} + \sigma^2_{\delta(L_4)_t}} \tag{11.7}$$

$$\delta(L_4)_{t,t-1} = (L_4)_t - (L_4)_{t-1} \tag{11.8}$$

where $t$ stands for the epoch number, $\omega$ is the weight factor related with epoch $t$. Note that the smoothed ionosphere measurements in Eq. (11.5) are still corrupted by the $DCB^i$ and $DCB_j$, which therefore should be estimated along with the ionosphere delay parameters.

Regardless of the second and third order of ionosphere refraction, the ionosphere delay can be expressed as follows [9]:

$$d_{ion} = \frac{40.28}{f^2} STEC \tag{11.9}$$

where $f$ stands for the carrier frequency, and $STEC$ stands for the slant total electron content along the signal path. Through substituting (11.9) into (11.3), and smoothing the $P_4$:

$$P_{4,s} = 40.28\left(\frac{1}{f_1^2} - \frac{1}{f_2^2}\right) STEC + DCB^i + DCB_j \tag{11.10}$$

The DCBs extracted from smoothed $P_4$ is more reliable.

## 11.3 Method to Model the Real-Time Spherical Harmonic Function and to Determine the DCBs

From (11.10), it is easy to get STEC, then VTEC:

$$STEC = -\frac{f_1^2 f_2^2}{40.28\left(f_1^2 - f_2^2\right)}\left(P_{4,s} - cDCB^i - cDCB_j\right) \tag{11.11}$$

$$VTEC = MF(z)STEC \tag{11.12}$$

$$MF = \cos\left(\arcsin\left(\frac{R}{R+H}\sin\left(\alpha z\right)\right)\right) \tag{11.13}$$

where $z$ is the satellite elevation angle, $R$ is the earth's radius, and $H$ is the altitude of the ionosphere thin shell. In order to accurately be compared with the results of CODE, the $H$ and $\alpha$ in this paper are references to CODE. This projection function is the best agreement with the projection of JPL Extended Slab Model [10].

CODE uses 15 order of spherical harmonic function to model the globe ionosphere products. Since for the regional area, the low order spherical harmonic function is much better, the spherical harmonic function model is shown as follows [11]:

$$E(\beta, s) = \sum_{n=0}^{\max\_n}\sum_{m=0}^{n}\tilde{P}_{nm}(\sin\beta)(a_{nm}\cos ms + b_{nm}\sin ms) \tag{11.14}$$

$$\tilde{P}_{nm} = \Lambda(n,m)P_{nm} = \sqrt{2\frac{2n+1}{1+\delta_{0m}}\frac{(n-m)!}{(n+m)!}}P_{nm} \tag{11.15}$$

where $\beta$ is the geocentric latitude of the ionosphere pierce point (IPP), $s = \lambda - \lambda_0$ is the sun-fixed longitude of the IPP, $\tilde{P}$ is normalized Legendre polynomial, $a_{nm}$, $b_{nm}$ are the spherical harmonic function model coefficients, max_$n$ is the maximum order, and $\delta$ is the Kronecker Delta. Substituting (11.11) and (11.12) into (11.14), the ionosphere spherical harmonic function model can be obtained:

$$\begin{aligned}&\sum_{n=0}^{\max\_n}\sum_{m=0}^{n}\tilde{P}_{nm}(\sin\beta)(a_{nm}\cos ms + b_{nm}\sin ms)\\ &= \cos\left(\arcsin\left(\tfrac{R}{R+H}\sin(\alpha z)\right)\right)\\ &-\left[\tfrac{f_1^2 f_2^2}{4028\left(f_1^2 - f_2^2\right)}\left(P_{4,s} - cDCB^i - cDCB_j\right)\right]\end{aligned} \tag{11.16}$$

where $a_{nm}$, $b_{nm}$, $DCB^i$, $DCB_j$ are unknown parameters to be estimated. During the estimating, with interval of two hours, the DCBs is considered as the same. In each period of time, a group of 25 coefficients in 4 order spherical harmonic function

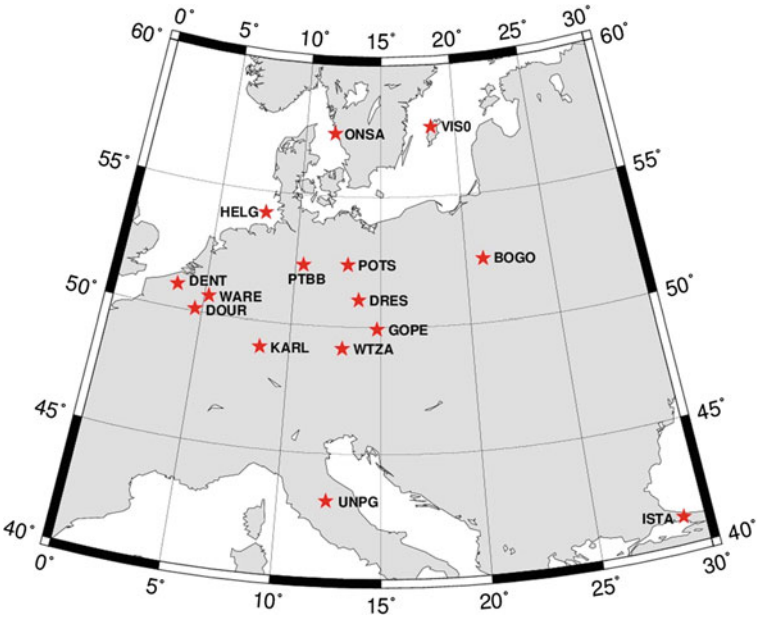


**Fig. 11.2** Distributions of IGS stations chosen

model coefficients as well as the DCBs of all the satellites and receivers participated in the estimation can be obtained. According to the Least Mean Square (LMS), it still needs a constraint condition as (11.17) to separate the satellites DCB:

$$\sum_{i=1}^{\max\_i} DCB^i = 0 \tag{11.17}$$

The weight matrix of adjustment stochastic model is unit weight which implies that the observations are of mutual independence.

## 11.4 Experiments and Results

### *11.4.1 Experiments Data*

15 evenly distributed IGS stations from Germany and its surrounding areas of April 9–18, 2012 (Day of Year: 100–109) are selected. A total of 10 days observations as the real time simulation data, the average distance among stations in the distribution intensive regions are about 200–300 km. With the real-time simulated data of the network, calculation once every 2 h in 10 continuous days is

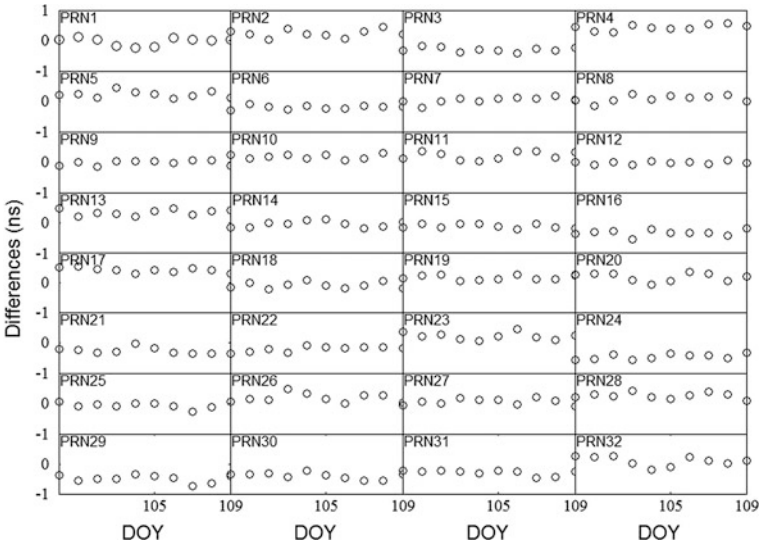


**Fig. 11.3** Differences in the satellites DCB value from this paper and CODE

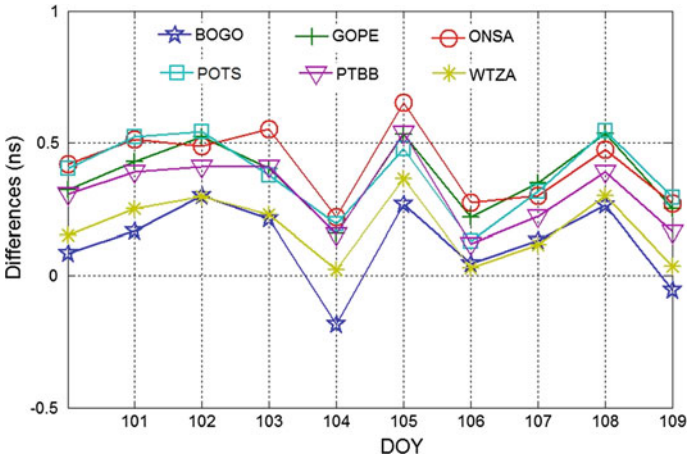


**Fig. 11.4** Differences in the receivers DCB value from this paper and CODE

conducted. Finally, the ionosphere spherical-harmonic model of the estimated area and the DCB of P1 to P2 are obtained and the results are compared with the results issued by CODE (Fig. 11.2).

**Table 11.1** The RMS and mean differences between satellite and receiver DCB estimates from April 9–18, 2012

| Satellite | RMS | Differences | Mean DCB of test | Satellite/ station | RMS | Differences | Mean DCB of test |
|---|---|---|---|---|---|---|---|
| PRN1 | 0.122 | −0.030 | −10.804 | PRN20 | 0.137 | 0.181 | 0.007 |
| PRN2 | 0.122 | 0.228 | 6.163 | PRN21 | 0.097 | −0.274 | 1.606 |
| PRN3 | 0.071 | −0.298 | −2.749 | PRN22 | 0.081 | −0.191 | 5.562 |
| PRN4 | 0.095 | 0.331 | −0.825 | PRN23 | 0.116 | 0.220 | 7.884 |
| PRN5 | 0.108 | 0.228 | 1.634 | PRN24 | 0.086 | −0.360 | −3.479 |
| PRN6 | 0.060 | −0.203 | −2.317 | PRN25 | 0.091 | −0.052 | −8.818 |
| PRN7 | 0.103 | 0.039 | 1.777 | PRN26 | 0.144 | 0.186 | −1.274 |
| PRN8 | 0.105 | 0.087 | −2.713 | PRN27 | 0.098 | 0.057 | −2.501 |
| PRN9 | 0.075 | −0.025 | −1.676 | PRN28 | 0.094 | 0.257 | 1.713 |
| PRN10 | 0.072 | 0.173 | −3.529 | PRN29 | 0.120 | −0.298 | 0.380 |
| PRN11 | 0.127 | 0.215 | 2.377 | PRN30 | 0.106 | −0.203 | −3.001 |
| PRN12 | 0.047 | −0.018 | 2.477 | PRN31 | 0.085 | 0.291 | 3.019 |
| PRN13 | 0.099 | 0.349 | 2.189 | PRN32 | 0.151 | 0.090 | −3.366 |
| PRN14 | 0.098 | −0.040 | 0.449 | BOGO | 0.147 | 0.124 | −3.567 |
| PRN15 | 0.067 | −0.105 | 1.133 | GOPE | 0.129 | 0.303 | 7.121 |
| PRN16 | 0.099 | −0.322 | 0.824 | ONSA | 0.137 | 0.408 | −5.411 |
| PRN17 | 0.079 | 0.309 | 1.952 | POTS | 0.140 | 0.428 | 6.433 |
| PRN18 | 0.101 | −0.094 | 1.703 | PTBB | 0.132 | 0.361 | −9.290 |
| PRN19 | 0.075 | 0.154 | 4.203 | WTZA | 0.120 | 0.180 | −8.960 |

### *11.4.2 DCBs Analysis*

As one of the analysis centers of IGS, CODE applies 15 orders Spherical Harmonic Function to model the globe TEC model, and has launched DCB of part of the IGS globe distributed stations and satellites (GPS & GLONASS). In this report, the CODE results are taken as reference. DCB values estimated by the authors and those released by CODE are compared, as shown in Figs. 11.3 and 11.4. The DCBs in the figures are the mean of 10 days. The vertical axis stands for biases, or differences (in nanoseconds) and the horizontal axis stands for the days of year in 2012. More details are displayed in Table 11.1.

Receiver DCB biases are basically less than 0.4 ns and those of the ONSA and POTS are 0.408 ns and 0.428 ns respectively. Since observations of them are found out that the number of valid observations for them is less than others each day from April 9–18, the larger bias in them are probably caused by fewer observations. Satellites DCB biases show good results which are all less than 0.35 ns. The RMS of all differences is lower than 0.2 ns. Considering that the order of Spherical Harmonic Function is 4 for regional area ionosphere, it turns out to be more sensitive which will also be approved in the next section.

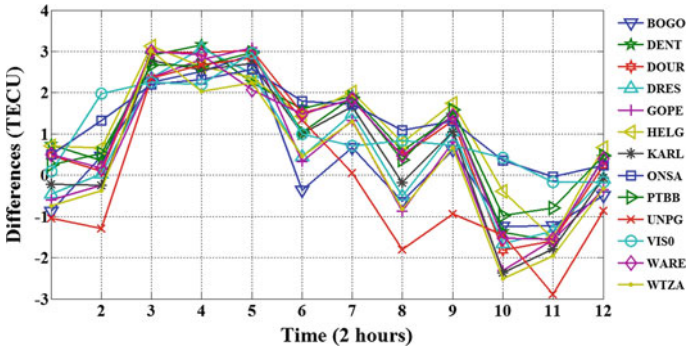


**Fig. 11.5** Differences in the stations VTEC value from this paper and CODE (100th day)

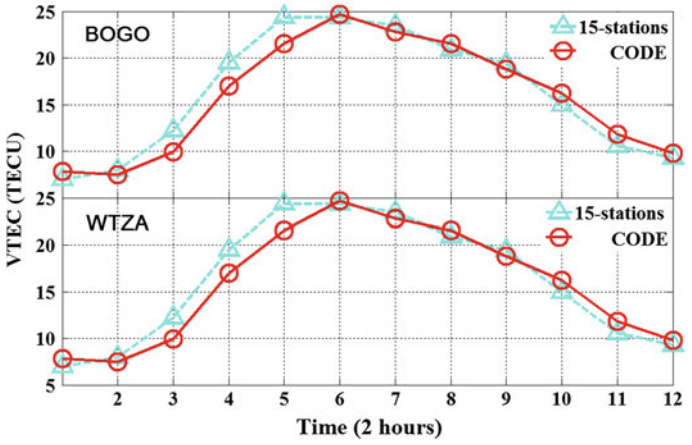


**Fig. 11.6** The VTEC of BOGO&WTZA in 100th day

### *11.4.3 DCBs Analysis*

During the estimation of real-time simulation, with interval of 2 h, VTEC data of 12 periods a day are obtained. Figure 11.5 shows the differences in all the stations VTEC per period in 100th day expect the ISTA for data anomalies. The single station VTEC per period is showed in Fig. 11.6. Due to space limitations, only BOGO and WTZA are in the figure. It shows that the differences of VTEC reach their peak value of 2–3 TECU at period 3–5, 10–11, and the rest are lower than 2TECU, especially the beginning and ending periods of which the differences reach less than 1TECU. The results show good agreement with CODE. From Fig. 11.6, the test values rise faster than CODE, and also decline faster. So it can conclude that the regional model can reflect better than globe model in which the differences are less than 3TECU. The distribution of stations net determines

effective number, density and geometric position of IPP and exercises a great influence on the accuracy of the ionosphere model. The average distance among stations in this paper is about 200–300 km and these stations are among the 30 degrees of latitude and 20 degrees of longitude, which is equivalent to the area from Beijing to Hong Kong in north-south direction and from Shanghai to Chengdu in east-west in China. However, the station distribution in CORS is more intensive in general. Therefore, the ionosphere model with higher accuracy can be achieved.

## 11.5 Summaries

The use of pseudorange and refined pseudorange to obtain the absolute electron content of the ionosphere, and then established regional ionosphere model is a common method. However, the determination of ionospheric delay by this method generally can not be used for precise positioning due to the precision problem. This paper use the part of global continuous tracking station to simulate aera CORS system. The effect of DCB is considered while estimating real-time regional Ionospheric modeling using spherical harmonic function, thereby the ionospheric model accuracy is improved. The comparative analytic results show that the method taken in this paper can effectively solve and exclude DCBs, and establish more accurate and sensitive real-time regional ionosphere model. It has important research significance of providing better ionosphere corrections information for single frequency receiver users by CORS network real-time monitoring of the CORS network changes of ionosphere.

## References

1. Gao Y, Liu ZZ (2002) Precise ionosphere modelling using regional GPS network data. J Glob Positioning Syst 1(1):18–24
2. Xiaoya Wang, Wenyao Zhu. Method and progress on monitoring ionospheric activity by GPS. Prog Astron 21(1):33–40
3. Schaer S (1995) Global and regional ionosphere models using the GPS double difference phase observable. IGS workshop. Potsdam
4. Xiaohong Z, Zhenghang L, Changsheng C (2001) Study on regional ionospheric model using dual-frequency GPS measurements. Geomat Inf Sci Wuhan Univ 26(2):140–143, 159
5. Yunbin Y (2002) Study on theories and methods of correcting ionosphere delay and monitoring ionosphere based on GPS. Institute of geodesy and geophysics. Chinese Academy of Science, China
6. Hongping Zhang (2006) Research on China area ionosphere monitoring and delay correction based on ground-based GPS. Shanghai astronomical observatory. Chinese Academy of Science, China
7. Gao Y, Heroux P, Kouba J (1994) Estimation of GPS receiver and satellite L1/L2 signal delay biases using data from CACS. In: Proceedings of KIS-94, Banff, Canada

8. Gao Y, Liao X, Liu ZZ (2002) Ionosphere modeling using carrier smoothed ionosphere observations from a regional GPS network. Geomatica 56(2):P97–P106
9. Zhenghang L, Jinsong H (2005) GPS surveying and data processing. Wuhan University Press, Wuhan
10. Zhenghang Li, Xiaohong Zhang (2009) New techniques and precise data processing methods of satellite navigation and positioning. Wuhan University Press, Wuhan
11. Jin R, Jin S, Feng G (2012) M_DCB: Matlab code for estimating GNSS satellite and receiver differential code biases. GPS solutions. Springer, China